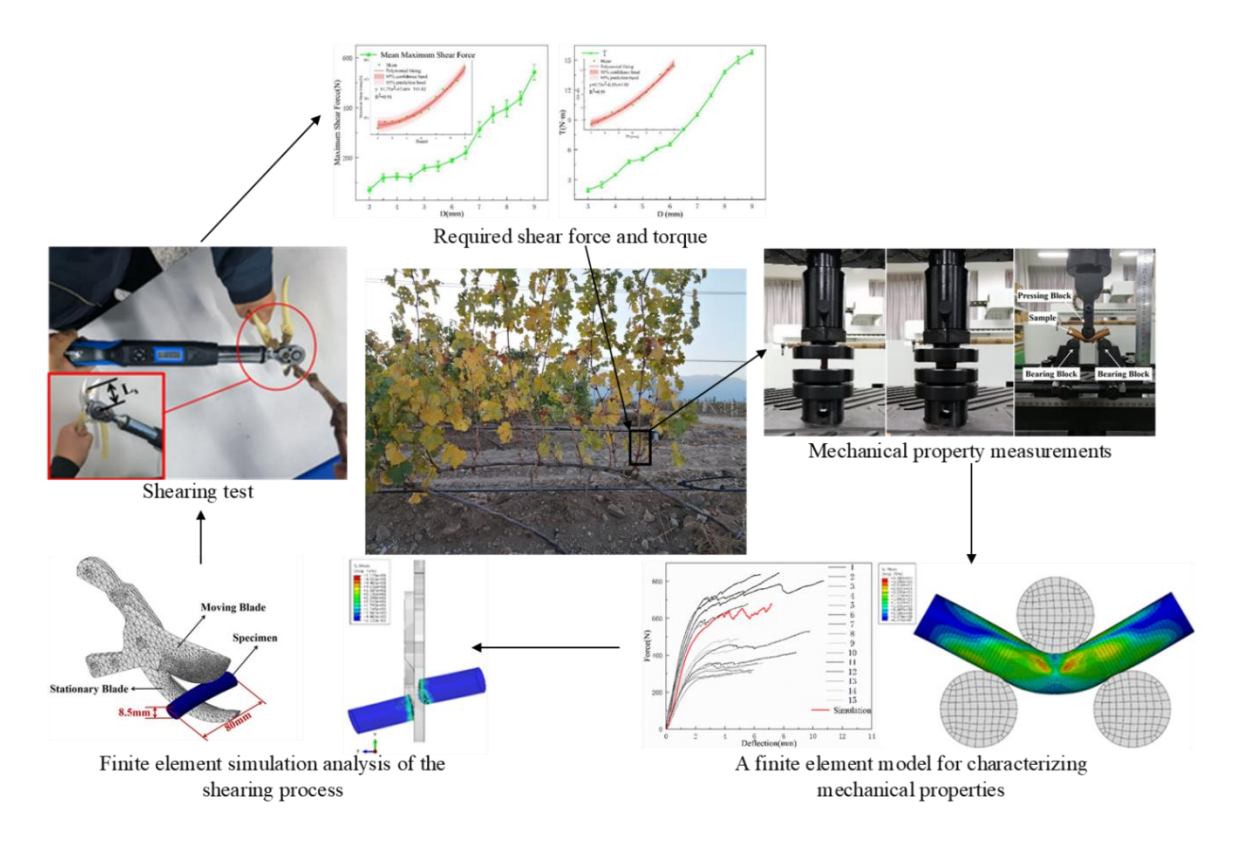
Investigating Shear Force and Torque of Grapevine Shoots Based on Experimental and Simulation Analysis

Lingxin Bu, Da Qiangqiang Zhang, Qianwen Kou, Yun Chen, Xingjia Li, Xingtao Wu, Teng Zhang, Xingrun Tang, Jipeng Wang, and Li Zhao A,*

*Corresponding author: linzhaoli@126.com

DOI: 10.15376/biores.20.3.6662-6679

GRAPHICAL ABSTRACT



Investigating Shear Force and Torque of Grapevine Shoots Based on Experimental and Simulation Analysis

Lingxin Bu, Da Qiangqiang Zhang, Qianwen Kou, Yun Chen, Xingjia Li, Xingtao Wu, Teng Zhang, Xingrun Tang, Jipeng Wang, and Li Zhao A

Winter pruning of grapevine branches is essential vineyard management, and knowledge of the biomechanical properties of branches is crucial for effective pruning. This study analyzed the dynamic behavior of grapevine shoots through axial-radial tensile, three-point bending, and shear tests. The axial elastic modulus, the radial elastic modulus, and the flexural modulus of grapevine shoots were 797 MPa, 79.8 MPa, and 5890 MPa, respectively. A finite element model of the grapevine shoot was established using the measured data, and a three-point bending simulation was conducted. The flexural modulus value obtained from the simulation was 5700 MPa, with a deviation of 3.37% from the experimental average, demonstrating the model's accuracy. Moreover, a mathematical regression model was developed to describe the relationship of the branch diameter with its maximum shear force and shear torque. Shear test simulations revealed the stress distribution during the shear process, with the maximum shear force and torque deviating 9.60% and 12.11%, respectively, from the experimental averages. This study provides data support for grapevine pruning automation. In the future, these findings may contribute to the development of automated mechanical pruning equipment for grapevines.

DOI: 10.15376/biores.20.3.6662-6679

Keywords: Grapevine branches; Simulation analysis; Axial—radial compression; Three-point bending; Shear test

Contact information: a: College of Mechatronic Engineering, North Minzu University, Yinchuan, Ningxia, 750021, China; b: School of Mechanical Engineering, Ningxia University, Yinchuan, Ningxia, 750021, China; *Corresponding author: linzhaoli@126.com

INTRODUCTION

In grapevine (*Vitis vinifera*), one of China's most important economic crops, pruned branches require proper handling, which is a critical aspect of agricultural production (Zahid *et al.* 2021). Currently, grapevine pruning relies on manual operations, which are inefficient, labor-intensive, and costly. The number of pruned branches is increasing with the continuous expansion of vineyard areas, further exacerbating the burden of manual pruning (Botterill *et al.* 2016). To address this issue, interdisciplinary research combining biomechanics and agricultural mechanization has become increasingly important (Sartori and Gambella 2014).

The application of biomechanics in agriculture, particularly in studying the mechanical properties of crops, provides a theoretical foundation for developing efficient and intelligent agricultural machinery (Bochtis *et al.* 2014; Chen *et al.* 2024). For example, investigating the mechanical characteristics of grapevine branches, including the relationship between shear force, diameter, and moisture content, is crucial for designing pruning robots tailored to grapevines (Silwal *et al.* 2022).

Automatic pruning of grapevines is a challenging task (Gentilhomme *et al.* 2023). However, improper pruning has detrimental effects on grapevine growth (Bruez *et al.* 2022), and the success of the pruning process depends on the accuracy of the shear force data. Romano *et al.* (2019) used a sensor array to determine the forces applied to pruning tools during grapevine branch cutting and found that the magnitude of the cutting force was primarily influenced by the branch diameter and moisture content. Sessiz *et al.* (2024) compared the shear force, energy, strength, and specific shear energy required to prune three local grapevine varieties using three blade shapes and obtained shear data under various conditions. Ozdemir *et al.* (2015) studied the cutting characteristics of wine grapevines and their relationships with moisture content, vine diameter, and variety and showed significant differences in the average cutting properties among varieties. Esgici *et al.* (2019) measured the cutting force and cutting energy by considering the grapevine branch diameter and vine age and revealed that both the cutting force and cutting energy increased with vine diameter and age.

The integration and enhancement of finite element software algorithms and visualization capabilities have improved the efficiency and accuracy of finite element analysis and expanded its biomechanics applications. Finite element analysis has proven effective in predicting the dynamic behavior of crops (Bu *et al.* 2020; Zulkifli *et al.* 2020; Ba *et al.* 2024). He *et al.* (2024) addressed low pruning efficiency by combining numerical simulation with experimental results to analyze data during the pruning process and designed a multifunctional grapevine branch-cutting machine that integrated cutting, picking, and collecting functions. Yang *et al.* (2022) employed a thinning algorithm and a lightweight convolutional neural network to detect winter pruning positions in Y-trellis cultivation systems and guide automated pruning equipment.

To facilitate the development of efficient and intelligent agricultural machinery, particularly grapevine pruning robots, this study integrated experimental measurements with numerical simulations to comprehensively analyze the key mechanical properties of grapevine branches—including radial and axial elastic moduli, flexural response, and shear force—thereby providing a theoretical foundation for system design and development. In addition, an effective finite element model was established to predict fracture behavior during three-point bending and shear tests of the grapevine branches. It was hypothesized that an adequate fit to the empirical data could be achieved by modeling of axial properties while assuming isotropic properties of the woody material in the xy plane, as a simplification. In addition, the simulation model did not consider the detailed microscturture of the wood, including lumens, annual rings, or microfibril angles, etc. The finite element simulations enabled a more precise assessment of the mechanical response of grapevine branches, providing scientific support for the design and optimization of pruning robots (You et al. 2023). These findings not only contribute to a deeper understanding of pruning mechanics in robotic systems, but also promote the intelligent advancement of grapevine pruning mechanization.

EXPERIMENTAL METHODS

Mechanical Property Measurements

Sample acquisition

The grapevine shoot samples used for the experiment were collected from 7- to 8-year-old Cabernet Sauvignon grapevines at a vineyard operated by the Mutong Winery Co., Ltd., in Ningxia, China (N38.61°, E106.13°). The growth conditions of the plants are shown in Fig. 1. The cordon was fixed to the cordon wire, and the upward-growing shoots were pruned and removed because the cordon had to be buried underground to survive the dry and cold winter. The samples were collected on November 1, 2023, with a wet-basis moisture content of $48.81 \pm 3.63\%$. All tests were completed within 1 day of sample collection.

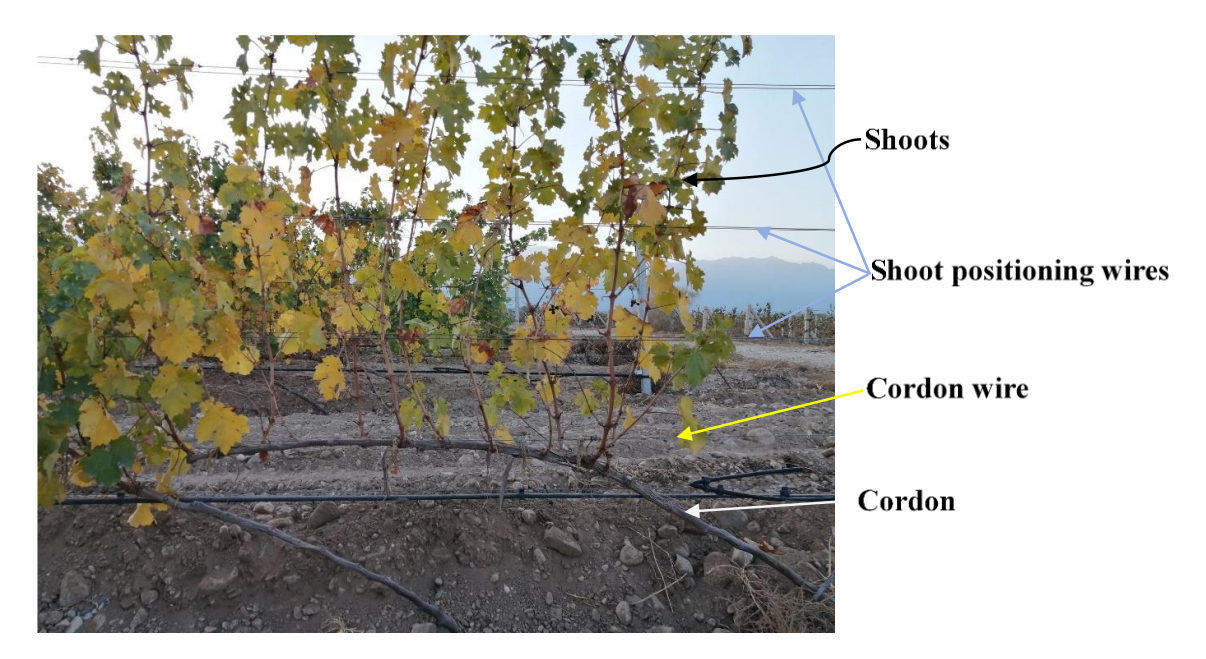


Fig. 1. Growth state of the grapevine

Compressive and Tensile Tests

An E45.105 electronic universal testing device (MTS Systems Co., Ltd., China) was used to conduct axial and radial compression tests on grapevine branches and measure the axial and radial elastic moduli (as shown in Fig. 2). The test speed was set to 1 mm min⁻¹. A total of 10 specimens were prepared for both the axial and radial compression tests, with an average diameter and length of 10 ± 0.2 mm.

The elastic behavior of grapevine branches occurs during the early stage of compression, which is reflected in the load-displacement curve as a linear increase in force with increasing displacement. The stress (σ_n) , strain (ε_n) , and elastic modulus (E) were calculated using Eqs. 1, 2, and 3, respectively,

$$\sigma_n = \frac{4F_n}{\pi d^2} \tag{1}$$

$$\varepsilon_n = \frac{\Delta l}{l_0} \tag{2}$$

$$E = \frac{\sigma_n}{\varepsilon_n} \tag{3}$$

where F_n is the test load (N); d is the specimen diameter (mm); $\triangle l$ is the rate of change in the specimen length; and l_0 is the nominal length of the sample prior to the test (mm).

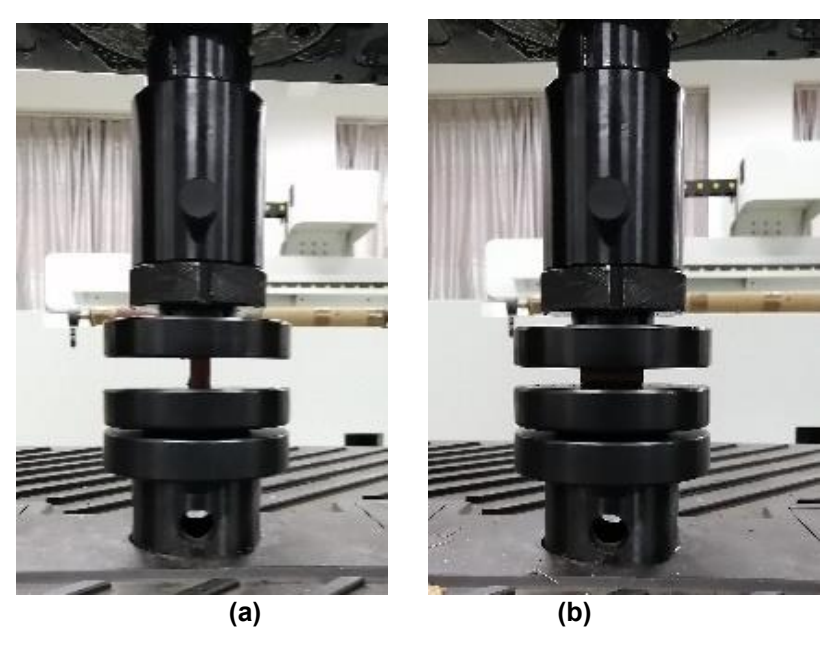


Fig. 2. Tests for elasticity modulus: (a) axial compression test and (b) radial compression test of a grapevine shoot sample

Three-point bending tests

The flexural modulus and bending strength of grapevine branches were determined using a three-point bending test. A total of 15 cylindrical grapevine branch samples, each with a length of 80 ± 10 mm, were used for this test. All tests were conducted using the electronic universal testing device described earlier. Each grapevine branch was positioned precisely on the support platform of the testing machine, ensuring that the center of the branch was aligned with the midpoint between two support points. The spacing between support points was set to 40 mm based on the length of the branches and the experimental requirements.

During the test, a loading head applied a vertical force to the grapevine branch at a constant speed, with the loading rate set to 1 mm min⁻¹, ensuring a smooth and controlled loading process. The experimental setup is illustrated in Fig. 3. The computer system recorded reaction force data in real time at a sampling frequency of 10 Hz. These data were used to calculate the flexural modulus and the mechanical properties of the branches using the stress–strain curve. The flexural modulus was determined using Eq. 4,

$$G_r = \frac{F\delta^3}{48I\gamma} \tag{4}$$

where I is the moment of inertia, $I = \pi d^4/64$ (mm⁴); d is the diameter of the samples (mm); and δ is the distance between the basement edges (mm).



Fig. 3. Three-point test of a grapevine shoot sample

Shearing tests

The force and torque required to cut grapevine branches were determined to provide theoretical support for the operation of pruning machine actuators. The selection of an appropriate force measurement sensor is crucial for the pruning torque test. Thus, a digital torque wrench (SLB-60R, 2–60 Nm, Sanliang, Dongguan) was used in this experiment to measure the torque during the shearing process. The manual pruning shears were integrated with the electric torque wrench and connected to a laptop *via* a data cable. The torque data collected by the electric torque wrench were transmitted to the computer and recorded, as shown in Fig. 4(a) (Igathinathane *et al.* 2011; Zahid *et al.* 2022). Grapevine branches were pretreated and prepared as samples with different diameters.

The aforementioned device was used to shear them and collect torque test data. A vernier caliper was used to measure each sample's diameter D (mm) and the distance from the sample to the scissors' rotation center. The maximum shear force during the cutting process was calculated using Eq. 5,

$$F_t = \frac{T}{L_S} \tag{5}$$

where F_t is the maximum shear force (N) of the sample; T is the maximum shear torque (Nm) of the sample; and L_s is the distance (m) between the sample and the center of rotation of the scissors. Five experimental tests were conducted for each diameter, as shown in Fig. 4(b).

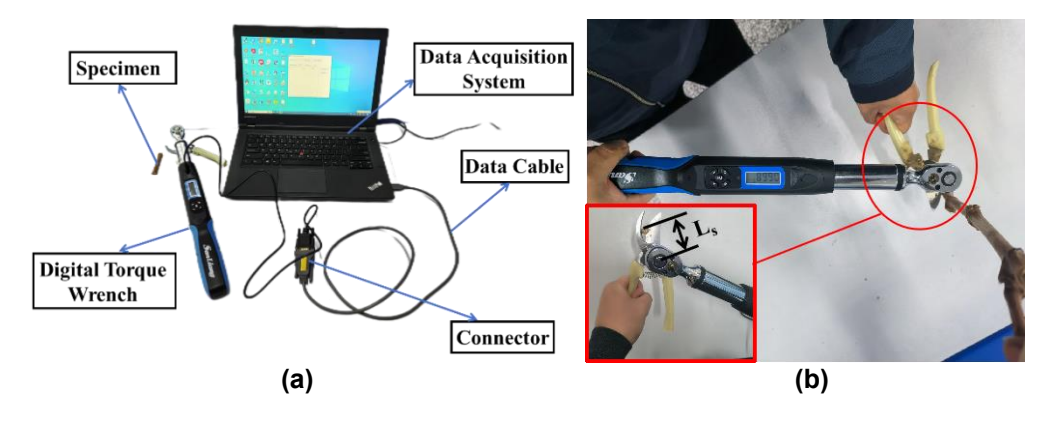


Fig. 4. Shearing test: (a) Overall setup; (b) Experimental process

Numerical Simulation

Numerical simulation of the three-point bending test

A finite element model of the pressing head and grapevine shoot was established to simulate the three-point bending test of grapevine shoot samples using ABAQUS finite element simulation software (version 2021, Dassault Systemes Simulia Corp., USA), as shown in Fig. 5. The grapevine shoot model was obtained by 3D reconstruction using a handheld 3D scanner (HANDYSCAN700, CreaForm, Canada). The simulation sample was extracted from the 3D reconstructed model. To ensure consistency with the three-point bending test conducted using the testing apparatus, both ends of the support heads were fixed, and a load was applied to the upper pressing head, which moved downward at a speed of 1 mm min⁻¹. The pressing block and support blocks consisted of 3810 C3D8R elements, while the grapevine sample contained 62,328 C3D8R elements. During the simulation process, element deletion was allowed when the elements failed. The damage parameters of the vine shoot samples are shown in Table 1. The model differentiated the axial properties of the woody material but for simplicity assumed equal properties in the other two primary directions at a submicroscopic scale.

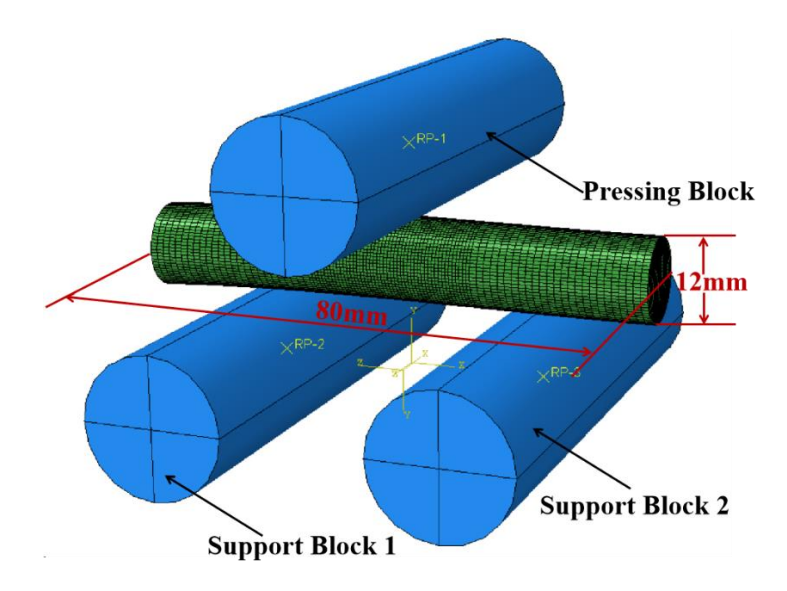


Fig. 5. Finite element model of the three-point bending simulation

Table 1. Damage Parameters of Grapevine Shoot Samples

Diameter (mm)	/ I ladion diam		Specific Energy (mJ mm ⁻²)	
12	0.04	14.47	72	

The grapevine shoot can be considered a transverse orthotropic material (Xie *et al.* 2020). The parameters used to describe the elasticity of the sample include the axial modulus (E_z), the radial modulus (E_r ; $E_r = E_x = E_y$), the flexural modulus on the anisotropic plane (G_r ; $G_r = G_{xz} = G_{yz}$), Poisson's ratio on the isotropic plane (μ_{xy}), and Poisson's ratio on the anisotropic plane (μ_r ; $\mu_r = \mu_{yz} = \mu_{xz}$) (Bu *et al.* 2021). The moduli of E_z and E_r were obtained from compression tests. The flexural modulus on the anisotropic plane G_r was determined using the three-point bending test. Because the test results do not directly provide values for the axial torsional shear modulus (G_{xy}) and Poisson's ratio on anisotropic

planes (μ_r), their values were estimated using Eqs. 6 and 7, respectively (Shen *et al.* 2015). The mechanical parameters of the sample and the testing tools used in the simulation are shown in Table 2. Equations 6 and 7 are given below:

$$G_{xy} = \frac{E_r}{2(1 + \mu_{xy})} \tag{6}$$

$$\mu_r < \frac{E_r}{E_z \sqrt{2\mu_{xy}}} \tag{7}$$

 Table 2. Material Properties of Grapevine Shoot Specimens and Test Tools

Materials	Density	Young's Modulus	Poisson's Ratio	Shear Modulus	
ivialeriais	(kg m ⁻³)	<i>E</i> (MPa)	μ	G (MPa)	
Camples	358	$E_r = 79.81$	$\mu_r = 0.15$	$G_r = 5887.41$	
Samples		$E_z = 797.11$	$\mu_{xy} = 0.4$	$G_{xy} = 51.06$	
Test tools	6720	7850	0.3	8×10 ⁴	

The plasticity of the specimen was described by Hill's quadratic yield criterion (Hill 1948; Kubík *et al.* 2023). Hill's potential function is an extension of the Mises function, which is expressed in terms of rectangular Cartesian stress components, as shown in Eq. 8,

$$f(\sigma) = \sqrt{F(\sigma_{22} - \sigma_{33})^2 + G(\sigma_{33} - \sigma_{11})^2 + H(\sigma_{11} - \sigma_{22})^2 + 2L\sigma_{23}^2 + 2M\sigma_{31}^2 + 2N\sigma_{12}^2}$$
(8)

where F, G, H, L, M, and N are constants obtained by tests of the material in different orientations, and their values are provided in Table 3.

Table 3. Hill's Plasticity Parameters (Šebek et al. 2020)

F	G	Н	L	M	N
2.1936	0.5841	-0.3341	0.3116	0.6173	0.4132

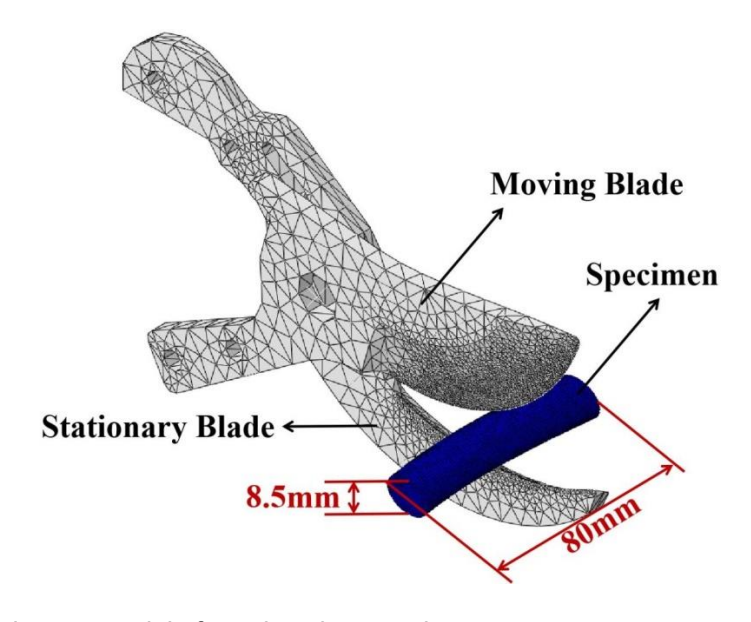


Fig. 6. Finite element model of pruning shear cutting

Numerical simulation of the shearing test

To determine the stress changes during the shear process of the specimen, a finite element model of the pruning shears and the specimen was established, as shown in Fig. 6. The shears were defined as a rigid body because the stiffness of the shear material was much greater than that of the specimen. The moving blade and stationary blade contained 8095 and 2697 C3D4 elements, respectively. The specimen was meshed into 16072 C3D8R elements. The stationary blade was fixed, and the rotation speed of the moving blade was set at 1 rad s⁻¹ for 0.5 s. Both the moving and stationary blade surfaces were in contact with the specimen, with a penalty of 0.3.

RESULTS

Axial Compression Test Results

Figure 7 presents the stress–strain curves obtained from compression tests on 10 selected grapevine samples. As illustrated, the stress–strain relationship of the grapevines exhibited a clear linear growth trend in the initial phase of the test. During this phase, as the strain increased, the stress on the sample increased, demonstrating typical elastic deformation characteristics. At this point, the slope of the curve represents the axial elastic modulus of the vine. Based on experimental data from 10 experiments, the average axial elastic modulus during the elastic phase was 797.11 ± 22.32 MPa, with a maximum of 844 MPa and a minimum of 771 MPa. The measured modulus range aligns with the mechanical characteristics of the porous, thin-walled cellular structures typically found in climbing plants (Gibson 2012). This value is substantially lower than that of dense hardwoods such as oak (about 10 GPa), indicating that grapevine branches are more prone to elastic deformation.

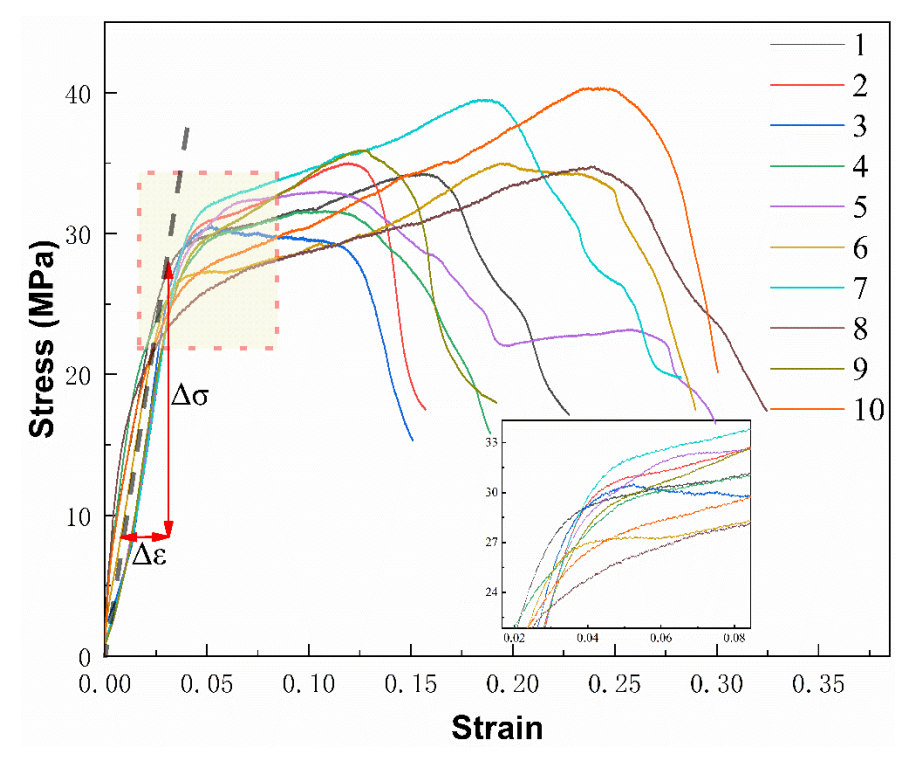


Fig. 7. Axial compression stress-strain curve diagram

As the compression load continued to be applied, the grapevine gradually approached its yield point and entered the plastic phase. In this phase, the curve began to flatten, indicating that the vine had entered the plastic deformation region, in which the material no longer fully recovered, resulting in permanent deformation. The average yield of the grapevine was 29.18 ± 1.78 MPa, with a maximum of 31.8 MPa and a minimum of 26.3 MPa among the 10 datasets. The occurrence of the yielding stage can be attributed to the plastic sliding of the microfibril network within the cell wall, as well as the buckling effect of the parenchymal cells (Keckes et al. 2003). This means that at this stress level, vine deformation is no longer elastic but has entered a state of plastic flow from which it cannot fully recover. Upon further loading, the stress value of the vine decreased as the strain continued to increase, eventually reaching the failure point and completely failing. At this point, the curve showed that the stress gradually decreased with increasing strain, indicating that the vine material failed after being subjected to stress beyond its maximum load-bearing capacity. This strain-softening behavior originates from the propagation of microcracks along the interface between the vascular bundles and the parenchyma tissue, as well as the collapse of the cell cavities (Niklas 1992). The appearance of the failure point signified that the structure of the grapevine had undergone irreversible damage, reached its strength limit, and was unable to withstand further external force.

Radial Compression Test Results

Figure 8 presents the stress–strain curves from radial compression tests on 10 grapevine samples.

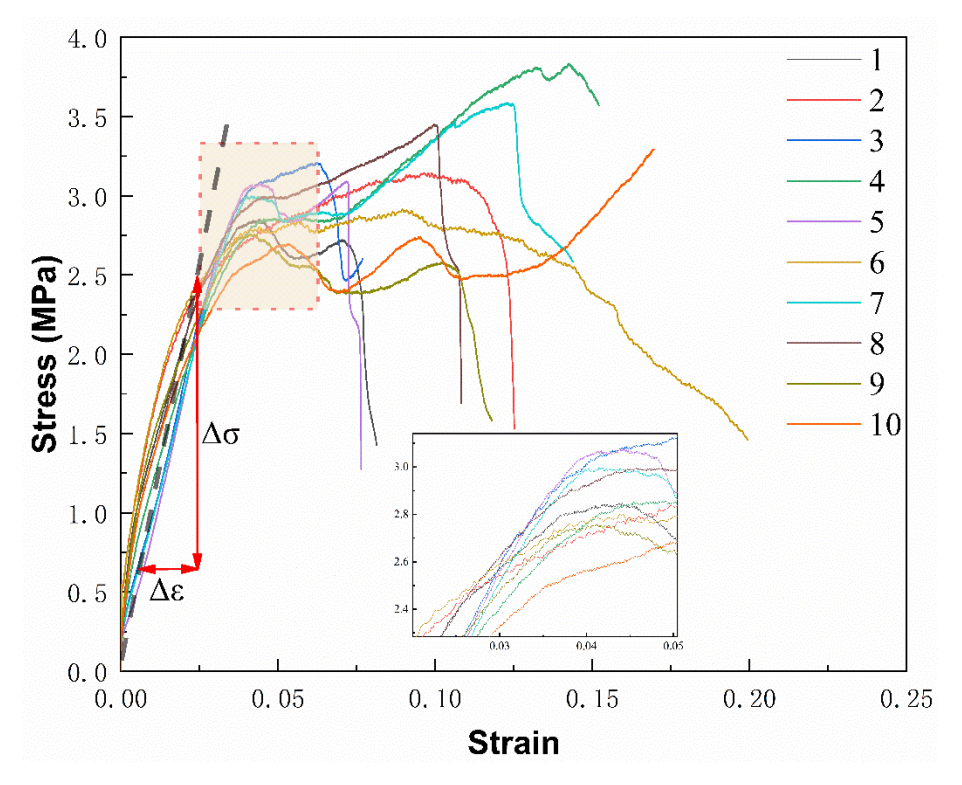


Fig. 8. Radial compression stress-strain curve

Initially, the curves showed a clear linear relationship between stress and strain, indicating that the stress increased uniformly with strain, demonstrating typical elastic

characteristics similar to the axial compression test. In this phase, the slope of the curve represented the radial elastic modulus of the vine. The experimental data revealed that the average radial elastic modulus during the elastic phase was 79.81 ± 5.35 MPa. This indicates that the vine exhibited linear elasticity under compression and could return to its original state upon removal of the external force. The radial elastic modulus was significantly lower than the axial value (797.11 ± 22.32 MPa). This difference originated from the anisotropic cellular structure of the grapevine: radial loading was perpendicular to the longitudinal axis of the vascular bundles, mainly causing the elastic compression of the thin-walled cell cavities rather than the stretching of cell walls (Niklas 1992).

As the compressive force increased, the grapevine approached its yield point and transitioned into the plastic deformation phase. In this phase, the slope of the curve began to decrease, showing that the vine was undergoing plastic deformation. At this point, the vine could not fully recover, and the deformation became irreversible. The stress value at the yield point was 2.87 ± 0.19 MPa. The extremely low yield strength is directly related to the rapid buckling failure of thin-walled cells under radial loading. When the cell cavity is compressed beyond the critical strain, the cell wall undergoes irreversible folding (Gibson et al. 2010). Beyond this point, the vine entered the nonlinear deformation stage, and the material underwent permanent deformation. With further loading, the stress decreased as the strain increased until the breaking point was reached, resulting in the complete failure of the vine. The fracture process is characterized by the disintegration of vascular bundles: under compressive loading, the parenchyma collapses, leaving the unsupported vascular bundles to fracture under bending stress (Niklas 1992). In this phase, the curve showed a trend of decreasing stress with increasing strain, indicating that the strength of the vine had reached its limit and that the material had undergone complete fracture or failure. The appearance of the breaking point signified that the material strength limit of the grapevine was reached and that it could not withstand any more stress.

Three-Point Bending Test Results

Figure 9(a) displays the stress–strain curves obtained from three-point bending tests on 15 grapevine samples.

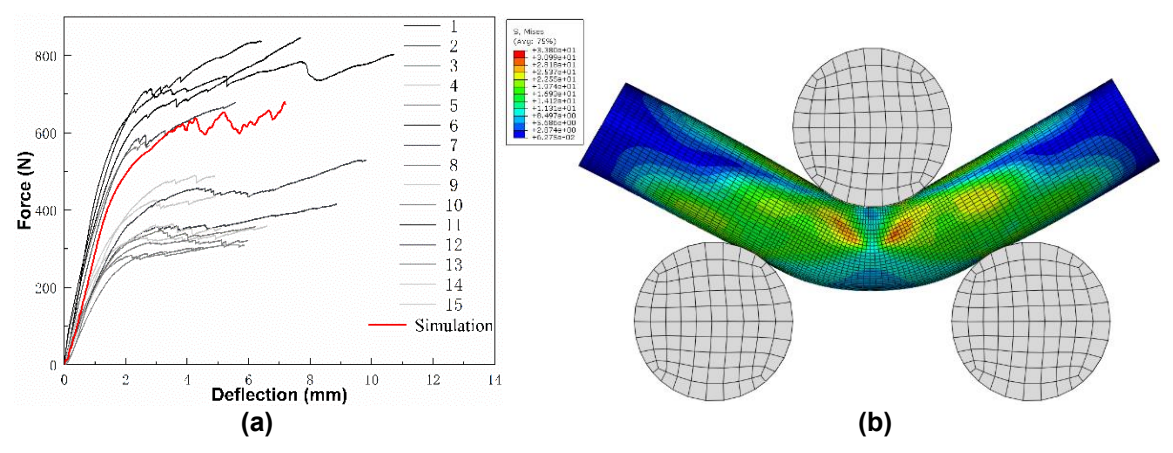


Fig. 9. Three-point bending test results: (a) Stress–strain curves from three-point bending tests; (b) Simulation results

The red curve represents the simulation data, while the other curves represent the 15 experimental datasets. Similar to axial and radial compression tests, the curves showed

both elastic and plastic deformation phases. For the 15 experiments, the average G_r value was 5887.41 \pm 380.92 MPa, with a minimum of 5227.85 MPa and a maximum of 6427.83 MPa. Figure 9(b) shows the results of the three-point bending test simulation. The simulated G_r value for the grapevines was 5695.43 MPa, with a relative deviation of 3.37%, which was within the acceptable error range. This indicates a high level of agreement between the experimental and simulation results, demonstrating the effectiveness and reliability of the numerical simulation method in predicting the mechanical properties of grapevines. These results provide valuable data and theoretical support for subsequent shear tests, reinforcing our understanding of grapevine mechanical behavior under various testing conditions.

Shearing Test Results

Figure 10 illustrates the effect of the grapevine sample diameter on its maximum shear force and shear torque. Figure 10(a) shows the maximum shear force values, and Fig. 10(b) shows the maximum torque values for different sample diameters. The red curve represents the fitted regression model, the light red area indicates the 95% confidence interval, and the pale pink area represents the 95% prediction interval. The relationships of the grapevine sample diameter with the maximum shear force (y_1) and maximum torque (y_2) followed a second-order polynomial, as shown in Eqs. 9 and 10. The fitting accuracy (R^2) values were 0.98 and 0.99, respectively, indicating excellent model precision. As the radius of the grapevine increased, both the maximum shear force and the required torque increased quadratically, demonstrating that thicker branches required greater shear force and torque. Equations 9 and 10 are as follows:

$$y_1 = 11.71x^2 - 67.66x + 191.82 (9)$$



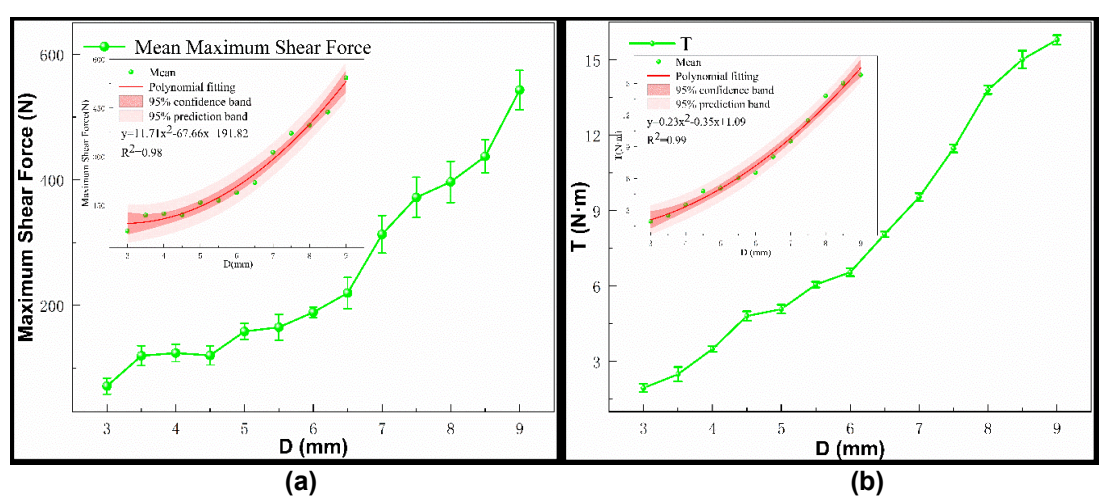


Fig. 10. Shear test results: (a) Maximum shear force values and (b) maximum shear torque values for samples with different diameters

The simulated shear test provided a more intuitive demonstration of the cutting process and the von Mises stress distribution in grapevine branches, as shown in Fig. 11. As the moving blade maintained contact with the grapevine model, stress at the contact position gradually increased until it exceeded the failure criterion. At this point, the mesh stiffness of the model began to decrease. Once it dropped to zero, the corresponding mesh

elements were deleted, with pruning shears representing the penetration into the grapevine model (as shown in Fig. 11(a)). As the moving blade continued to rotate, significant stress changes occurred along the sheared surface. Both the moving and fixed blades penetrated the sample until complete separation occurred at approximately 0.4 seconds (as shown in Fig. 11(b)–(d)). During the entire shear process, the maximum von Mises stress experienced by the sample was 59.29 MPa at t = 0.31 s.

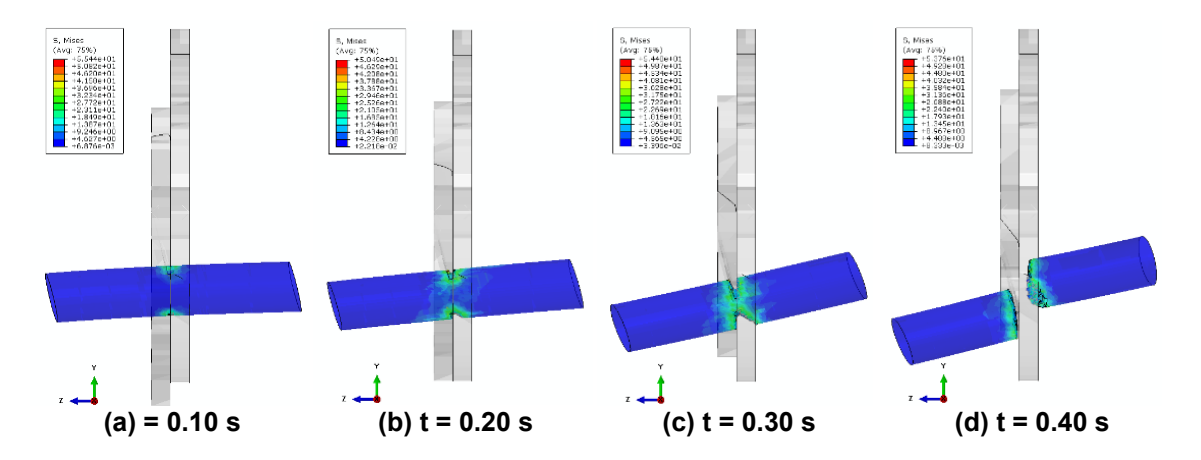


Fig. 11. Shear process of the sample

Figure 12 shows the variations in shear force and shear torque over time during the simulation. The shear force and shear torque exhibited the same trend, increasing continuously after the scissors made contact with the sample and reaching maximum values of 395 N and 13.2 Nm, respectively, at 0.31 s. The deviations from the experimental averages ($F_{mean} = 437$ N, $T_{mean} = 15.0$ Nm) were 9.6% and 12.1%, respectively. The simulation results indicate that the established finite element model could be used to predict the stress distribution and estimate the shear force and torque required for cutting branches.

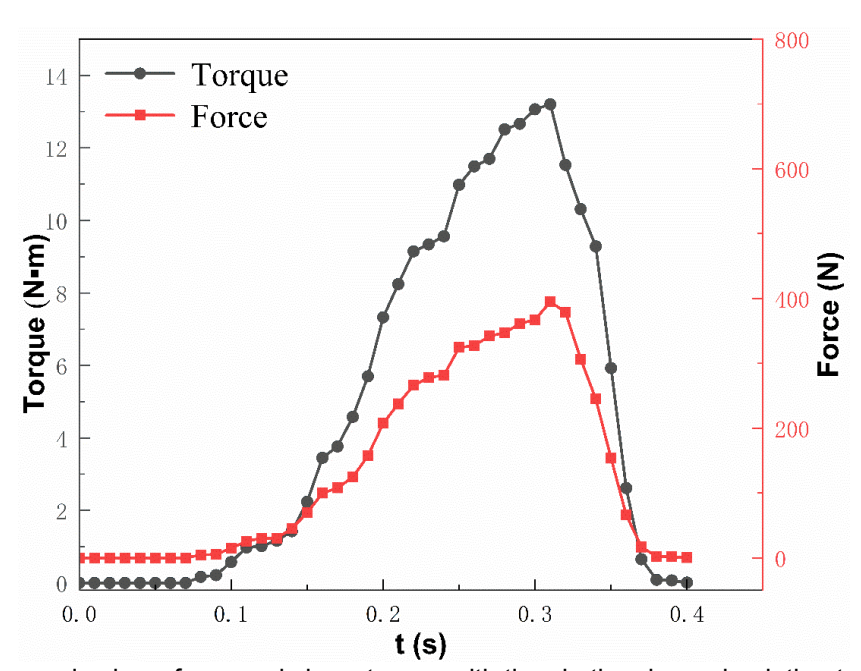


Fig. 12. Changes in shear force and shear torque with time in the shear simulation test

DISCUSSION AND ANALYSIS

Many wood samples derived from large logs, such as spruce (Nečemer et al. 2025) and beech (Zlámal et al. 2024), are generally treated as orthotropic materials. Due to the orientation of wood grain and variability in sampling positions, these materials exhibit distinct mechanical properties along the longitudinal, radial, and tangential directions. In contrast, slender branches from species such as peach (Song et al. 2025), apple (Bu et al. 2021), and jujube trees (Wang et al. 2020) typically have nearly circular cross-sections with small diameters perpendicular to the axial direction. The mechanical properties along orthogonal directions in the cross-section are largely similar. Notably, Wang et al. (2020) used CT scanning to reconstruct the internal microstructure of jujube branches and demonstrated, through both simulations and experiments, that the radial and tangential mechanical properties are nearly identical. Thus, modeling slender branches as transversely orthotropic materials is a reasonable and practical simplification. Furthermore, some researchers have attempted to establish a correlation between the plant microstructure and their macroscopic mechanical properties to explain the mechanical behavior under natural loading conditions (Wu et al. 2010; Horbens et al. 2015). Microscopic structures, such as microfibrillar angles and cell wall structures, can indeed enhance the model and control the mechanics to behave more precisely. However, from an engineering perspective, greater emphasis is placed on macroscopic properties such as the elastic modulus and strength limits of materials.

The measured axial elastic modulus (E_z) and radial elastic modulus (E_r) of grapevine branches were 797.11 \pm 22.32 MPa and 79.81 \pm 5.35 MPa, respectively. Compared with other fruit tree branches (as shown in Table 4), both E_z and E_r values are higher than those reported for peach and apple branches but lower than those reported for jujube trunks and branches. For the flexural modulus (G_r) , the measured value was 5887.41 \pm 380.92 MPa, approximately 10.8 times greater than that of the peach branch. This substantial difference highlights the mechanical variability among branch materials across different tree species. Even within the same species, such as jujube, mechanical properties may differ greatly across cultivars. For instance, the E_z reported by Wang et al. (2020) (4270 MPa) is about 7.45 times higher than that of the winter jujube branch reported by Zheng et al. (2024) (573 MPa). Moreover, plant moisture content significantly affects biomechanical properties (Yang et al. 2016). Due to the local arid climate, the grapevine branches in this study had a wet-basis moisture content of 48.8% at testing, which was lower than the 59.6% reported by Rodríguez-González et al. (2020). This reduced moisture content corresponds to higher bending strength and modulus of elasticity (Dadzie et al. 2016), which explains the relatively high values of E_z , E_r , and G_r that were obtained.

The shear force and torque of branches are critical parameters in the design of pruning mechanisms. When pruning shears are used as end-effectors, shear force and torque testing assist in motor selection (Silwal *et al.* 2022). The testing methodology employed in this study is consistent with that of Zahid *et al.* (2022), which was developed for apple pruning robot end-effector design. The results showed a significant regression relationship between the maximum shear force and branch diameter, as illustrated in Fig. 10(a). As the cutting diameter increased from 3 to 9 mm, the average shear force rose from 71.2 to 437.0 N, consistent with the findings of Goksel (2024). Furthermore, shear testing using a universal testing machine enables the exploration of the effects of cutting angle (Xie *et al.* 2022) and blade geometry (Sessiz *et al.* 2024) on cutting force. Optimizing shear blade design and cutting strategies represents a promising direction for future research. In

addition to pruning shears, disc blades are also considered potential candidates for end-effectors (Qiu *et al.* 2021; Meng *et al.* 2019). The maximum torque measured in this study (as shown in Fig. 10(b)), along with the developed finite element model, can be applied to evaluate the feasibility of disc-saw cutting systems.

Table 4. Mechanical Parameters of Several Fruit Tree Branches

Material	Radial elastic modulus <i>E</i> _r (MPa)	Axial elasticity modulus E _z (MPa)	Axial torsional shear modulus G _{xy} (MPa)	Flexural	Poisson's ratio on anisotropic plants μr	Poisson's ratio for isotropic plants μ_{xy}
Peach branch (Song <i>et al.</i> 2025)	25.94 ± 1.90	186.76±17.54	9.61 ± 0.71	546.05 ± 25.66	0.166	0.35
Apple branch (Bu <i>et al</i> . 2021)	29.81 ± 4.02	181.69±17.88	10.65	337.05 ± 66.52	0.2	0.4
Winter jujube trunk (Zheng <i>et</i> <i>al</i> . 2024)	69.92 ± 5.80	1048.63 ± 70.14	24.97 ± 2.23	26.72 ± 2.04	0.08	0.3
Winter jujube branch (Zheng et al. 2024)	83.29 ± 2.46	572.55 ± 14.04	32.04 ± 0.95	28.97 ± 2.79	0.16	0.3
Jujube branch (Wang et al. 2020)	357.08	4266.20	46.93	162.12	0.23	0.35

CONCLUSIONS

Current scientific reports severely lack foundational research on the mechanical properties of grapevine branches, leading to a lack of a theoretical basis for the design of grapevine pruning machines. Therefore, axial—radial tension tests, three-point bending tests, and shear tests were conducted. The conclusions were as follows:

1. Through axial—radial compression tests on grapevine branches, the axial elastic modulus was determined (E_z) to be 797.11 ± 22.32 MPa, with a yield stress of 29.18 ± 1.78 MPa. The radial elastic modulus (E_r) was 79.81 ± 5.35 MPa, with a yield stress of 2.87 ± 0.19 MPa. The three-point bending test determined the flexural modulus (G_r) to be 5887.41 ± 380.92 MPa. A finite element model of the grapevine was established based on the measured data, and the three-point bending simulation test yielded a

- flexural modulus value of 5670 MPa, with a deviation of 3.4% from the experimental average, indicating good model accuracy.
- 2. A mathematical model was established using shear tests to relate the grapevine branch diameter to the maximum shear force and required shear torque. Based on the established finite element model, a branch shear simulation test was conducted to determine the stress distribution during grapevine cutting. The deviations of the maximum shear force and torque from the experimental averages were 9.6% and 12.1%, respectively, indicating that the model could predict the stress distribution and estimate the shear force and torque required for branch cutting.

ACKNOWLEDGMENTS

The authors are grateful for the support of the Natural Science Foundation of Ningxia, grant number 2023AAC03302 and North Minzu University, grant number 2021KYQD31.

REFERENCES CITED

- Ba, S., Ban, Y., Lyu, K., Liu, Y., Wen, J., and Li, W. (2024). "Finite element explicit dynamics simulation of an impact cutting mechanism analysis of *Populus tomentosa* branches," *BioResources* 19(2), 3614-3636. DOI: 10.15376/biores.19.2.3614-3636
- Bochtis, D. D., Sørensen, C. G. C., and Busato, P. (2014). "Advances in agricultural machinery management: A review," *Biosystems Engineering* 126, 69-81. DOI: 10.1016/j.biosystemseng.2014.07.012
- Botterill, T., Paulin, S., Green, R., Williams, S., Lin, J., Saxton, V., Mills, S., Chen, X., and Corbett-Davies, S. (2016). "A robot system for pruning grape vines," *Journal of Field Robotics* 34, 1100-1122. DOI: 10.1002/rob.21680
- Bruez, E., Cholet, C., Giudici, M., Simonit, M., Martignon, T., Boisseau, M., Weingartner, S., Poitou, X., Rey, P., and Geny-Denis, L. (2022). "Pruning quality effects on desiccation cone installation and wood necrotization in three grapevine cultivars in France," *Horticulturae* 8, article 681. DOI: 10.3390/horticulturae8080681
- Bu, L., Chen, C., Hu, G., Zhou, J., Sugirbay, A., and Chen, J. (2021). "Investigating the dynamic behavior of an apple branch-stem-fruit model using experimental and simulation analysis," *Computers and Electronics in Agriculture* 186, article ID 106224. DOI: 10.1016/j.compag.2021.106224
- Bu, L., Hu, G., Chen, C., Sugirbay, A., and Chen, J. (2020). "Experimental and simulation analysis of optimum picking patterns for robotic apple harvesting," *Scientia Horticulturae* 261, article ID 108937. DOI: 10.1016/j.scienta.2019.108937
- Chen, X., Wang, W., He, X., Liu, F., Li, C., and Wu, S. (2024). "Analysis of the mechanical interaction force between the reel and wheat plants and prediction of wheat biomass," *Biosystems Engineering* 246, 67-81. DOI: 10.1016/j.biosystemseng.2024.07.013
- Dadzie, P., Amoah M., Frimpong-Mensah K., and Inkum, P. (2016). "Variation in bending strength properties in stem and branch woods as influenced by density and

- moisture levels in *Entandrophragma cylindricum*," *Australian Forestry* 79, 233-240. DOI:10.1080/00049158.2016.1251816
- Esgici, R., Pekitkan, F. G., Ozdemir, G., Guzel, E., and Sessiz, A. (2019). "Cutting parameters of some grape varieties subject to the diameter and age of canes," *Fresenius Environmental Bulletin* 28, 167-170.
- Gentilhomme, T., Villamizar, M., Corre, J., and Odobez, J. M. (2023). "Towards smart pruning: ViNet, a deep-learning approach for grapevine structure estimation," *Computers and Electronics in Agriculture* 207, article ID 107736. DOI: 10.1016/j.compag.2023.107736
- Gibson, L. (2012). "The hierarchical structure and mechanics of plant materials," *Journal of The Royal Society Interface* 9, 2749-2766. DOI: 10.1098/rsif.2012.0341
- Gibson, L., Ashby, M., Harley, B. (2010). *Cellular Materials in Nature and Medicine*, Cambridge University Press.
- Goksel, P. (2024). "Mechanical properties of okuzgozu (*Vitis vinifera L. cv.*) grapevine canes," *Journal of King Saud University Science* 36, article ID 103034. DOI: 10.1016/j.jksus.2023.103034
- He, L., Wang, Z., Song, L., Bao, P., and Cao, S. (2024). "Simulation and testing of grapevine branch crushing and collection components," *Agriculture* 14, article 1583. DOI: 10.3390/agriculture14091583
- Hill, R. (1948). "A theory of the yielding and plastic flow of anisotropic metals," *Proceedings of the Royal Society of London. Series A. Mathematical and Physical Sciences* 193, 281-297.
- Horbens, M., Branke, D., Gartner, R., Voigt, A., Stenger, F., and Neinhuis, C. (2015). "Multi-scale simulation of plant stem reinforcement by brachysclereids: A case study in apple fruit peduncles," *Journal of Structural Biology* 192, 116-126. DOI: 10.1016/j.jsb.2015.08.002
- Igathinathane, C., Pordesimo, L. O., Schilling, M. W., and Columbus, E. P. (2011). "Fast and simple measurement of cutting energy requirement of plant stalk and prediction model development," *Industrial Crops and Products* 33, 518-523. DOI: 10.1016/j.indcrop.2010.10.015
- Keckes, J., Burgert, I., Frühmann, K., Müller, M., Kölln, K., Hamilton, M., Burghammer, M., Roth, S., Stanzl-Tschegg, S., and Fratzl, P. (2003). "Cell-wall recovery after irreversible deformation of wood," *Nature Materials* 2, 810-813. DOI: 10.1038/nmat1019
- Kubík, P., Šebek, F., Krejčí, P., Brabec, M., Tippner, J., Dvořáček, O., Lechowicz, D., and Frybort, S. (2023). "Linear woodcutting of European beech: Experiments and computations," *Wood Science and Technology* 57, 51-74. DOI: 10.1007/s00226-022-01442-6
- Meng, Y., Wei, J., Wei, J., Chen, H., and Cui, Y. (2019). "An ANSYS/LS-DYNA simulation and experimental study of circular saw blade cutting system of mulberry cutting machine," *Computers and Electronics in Agriculture* 157, 38-48. DOI: 10.1016/j.compag.2018.12.034
- Nečemer, B., Fakin, J., Glodež, S., Šraml, M., Klemenc, J., and Fajdiga, G. (2025). "Bending quasi-static and fatigue behaviour of Norway spruce wood using experimental approach and FEM analysis," *Case Studies in Construction Materials* 22, article ID e04734. DOI: 10.1016/j.cscm.2025.e04734
- Niklas, K. (1992). *Plant Biomechanics: An Engineering Approach to Plant Form and Function*, University of Chicago press.

- Ozdemir, G., Sessiz, A., Esgici, R., and Elicin, A. K. (2015). "Cutting properties of wine grape cultivars," *Scientific Papers. Series B, Horticulture*. LIX, 151-158.
- Qiu, M., Meng, Y., Li, Y., Shen, X. (2021). "Sugarcane stem cut quality investigated by finite element simulation and experiment," *Biosystems Engineering* 206, 135-149. DOI: 10.1016/j.biosystemseng.2021.03.013
- Rodríguez-González, Á., Casquero, P.A., Carro-Huerga, G., García-González, J., Álvarez-García, S., Juan-Valdés, A. (2020). "Failure under stress of grapevine wood: The effects of the cerambycid *Xylotrechus arvicola* on the biomechanics properties of Vitis vinifera," *Maderas. Ciencia y Tecnología* 22, 167-178. DOI: 10.4067/S0718-221X2020005000203
- Romano, E., Caruso, L., Longo, D., Vitale, E., Schillaci, G., and Rapisarda, V. (2019). "Investigation of hand forces applied to a pruning tool Pilot study," *Annals of Agricultural and Environmental Medicine* 26, 472-478. DOI: 10.26444/aaem/109751
- Sartori, L., and Gambella, F. (2014). "Comparison of mechanical and manual cane pruning operations on three varieties of grape (Cabernet Sauvignon, Merlot, and Prosecco) in Italy," *Transactions of the ASABE* 57, 701-707. DOI: 10.13031/trans.57.10446
- Šebek, F., Kubík, P., Brabec, M., and Tippner, J. (2020). "Modelling of impact behaviour of European beech subjected to split Hopkinson pressure bar test," *Composite Structures* 245, article ID 112330. DOI: 10.1016/j.compstruct.2020.112330
- Sessiz, A., Ozdemir, G., and Eliçin, A. K. (2024). "Shear tests of grapevine (*Vitis vinifera* L.) canes," in: *15th International Congress on Agricultural Mechanization and Energy in Agriculture*, Springer Nature, Cham, Switzerland, pp. 39-50.
- Shen, C., Li, X., Tian, K., Zhang, B., Huang, J., and Chen, Q. (2015). "Experimental analysis on mechanical model of ramie stalk," *Transactions of the Chinese Society of Agricultural Engineering* 31, 26-33. DOI: 10.11975/j.issn.1002-6819.2015.20.004
- Silwal, A., Yandun, F., Nellithimaru, A., Bates, T., and Kantor, G. (2022). "Bumblebee: A path towards fully autonomous robotic vine pruning," *Field Robotics* 2, 1661-1696. DOI: 10.55417/fr.2022051
- Song, H., Wang, K., Wang, Y., and Zhang, X. (2025). "Study on the abscission mechanical model of the peach fruit-branch system based on a mixed-mode cohesive zone model and finite element method," *Computers and Electronics in Agriculture* 231, article ID 109965. DOI: 10.1016/j.compag.2025.109965
- Wang, B., He, M., Li, C., Wang, L., and Meng, H. (2020). "Microstructure and biomechanical characterisation of jujube branches," *Biosystems Engineering* 194, 165-176. DOI: 10.1016/j.biosystemseng.2020.04.004
- Wu, Y., Wang, S., Zhou, D., Xing, C., Zhang, Y., and Cai, Z. (2010). "Evaluation of elastic modulus and hardness of crop stalks cell walls by nano-indentation," *Bioresource Technology* 101, 2867-2871. DOI: 10.1016/j.biortech.2009.10.074
- Xie, L., Wang, J., Cheng, S., and Du, D. (2020). "Cutting characteristics of sugarcane in terms of physical and chemical properties," *Transactions of the ASABE* 63, 1007-1017. DOI: 10.13031/trans.13859
- Xie, L., Wang, P., Luo, J., Yi, W., and Deng, J. (2022). "Optimisation and numerical simulation of shearing blade used for citrus seedling grafting," *Biosystems Engineering* 215, 67-79. DOI: 10.1016/j.biosystemseng.2022.01.006
- Yang, Q., Yuan, Y., Chen, Y., and Xun, Y. (2022). "Method for detecting 2D grapevine winter pruning location based on thinning algorithm and lightweight convolutional

- neural network," *International Journal of Agricultural and Biological Engineering* 15, 177-183. DOI: 10.25165/j.ijabe.20221503.6750
- Yang, Y., Chen, L., Li, N., and Zhang, Q. (2016). "Effect of root moisture content and diameter on root tensile properties," *Plos One* 11, article ID e0151791. DOI: 10.1371/journal.pone.0151791
- You, A., Parayil, N., Krishna, J. G., Bhattarai, U., Sapkota, R., Ahmed, D., Whiting, M., Karkee, M., Grimm, C. M., and Davidson, J. R. (2023). "Semiautonomous precision pruning of upright fruiting offshoot orchard systems: An integrated approach," *IEEE Robotics & Automation Magazine* 30, 10-19. DOI: 10.1109/MRA.2023.3309098
- Zahid, A., Mahmud, M. S., He, L., Heinemann, P., Choi, D., and Schupp, J. (2021). "Technological advancements towards developing a robotic pruner for apple trees: A review," *Computers and Electronics in Agriculture* 189, article ID 106383. DOI: 10.1016/j.compag.2021.106383
- Zahid, A., Mahmud, M. S., He, L., Schupp, J., Choi, D., and Heinemann, P. H. (2022). "An apple tree branch pruning analysis," *HortTechnology* 32, 90-98. DOI: 10.21273/HORTTECH04924-21
- Zheng, Z., Hu, Y., Dong, J., Zhao, P., Liu, Y., Jiang, X., Qiao, Y., Sun, S., and Huang, Y. (2024). "Characterising vibration patterns of winter jujube trees to optimise automated fruit harvesting," *Biosystems Engineering* 248, 255-268. DOI: 10.1016/j.biosystemseng.2024.11.004
- Zlámal, J., Mařík, R., Vojáčková, B., Cristini, V., Brabec, M., Praus, L., and Tippner, J. (2024). "Elasto-plastic material model of green beech wood," *Journal of Wood Science* 70, article 29.
- Zulkifli, N., Hashim, N., Harith, H. H., and Mohamad Shukery, M. F. (2020). "Finite element modelling for fruit stress analysis A review," *Trends in Food Science and Technology* 97, 29-37. DOI: 10.1016/j.tifs.2019.12.029

Article submitted: April 21, 2025; Peer review completed: May 29, 2025; Revised version received and accepted: June 16, 2025; Published: June 24, 2025. DOI: 10.15376/biores.20.3.6662-6679